Computing and Partitioning Cloud Feedbacks Using Cloud Property Histograms. Part II: Attribution to Changes in Cloud Amount, Altitude, and Optical Depth

MARK D. ZELINKA

Department of Atmospheric Sciences, University of Washington, Seattle, Washington, and Program for Climate Model Diagnosis and Intercomparison, Lawrence Livermore National Laboratory, Livermore, California

STEPHEN A. KLEIN

Program for Climate Model Diagnosis and Intercomparison, Lawrence Livermore National Laboratory, Livermore, California

DENNIS L. HARTMANN

Department of Atmospheric Sciences, University of Washington, Seattle, Washington

(Manuscript received 12 May 2011, in final form 15 November 2011)

ABSTRACT

Cloud radiative kernels and histograms of cloud fraction, both as functions of cloud-top pressure and optical depth, are used to quantify cloud amount, altitude, and optical depth feedbacks. The analysis is applied to doubled-CO_2 simulations from 11 global climate models in the Cloud Feedback Model Intercomparison Project.

Global, annual, and ensemble mean longwave (LW) and shortwave (SW) cloud feedbacks are positive, with the latter nearly twice as large as the former. The robust increase in cloud-top altitude in both the tropics and extratropics is the dominant contributor to the positive LW cloud feedback. The negative impact of reductions in cloud amount offsets more than half of the positive impact of rising clouds on LW cloud feedback, but the magnitude of compensation varies considerably across the models. In contrast, robust reductions in cloud amount make a large and virtually unopposed positive contribution to SW cloud feedback, though the intermodel spread is greater than for any other individual feedback component. Overall reductions in cloud amount have twice as large an impact on SW fluxes as on LW fluxes, such that the net cloud amount feedback is moderately positive, with no models exhibiting a negative value. As a consequence of large but partially offsetting effects of cloud amount reductions on LW and SW feedbacks, both the mean and intermodel spread in net cloud amount feedback are smaller than those of the net cloud altitude feedback. Finally, the study finds that the large negative cloud feedback at high latitudes results from robust increases in cloud optical depth, not from increases in total cloud amount as is commonly assumed.

1. Introduction

Since the early days of climate modeling, it has been recognized that changes in clouds that accompany climate change provide a feedback through their large impact on the radiation budget of the planet. Schneider and Dickinson (1974) noted that accurate assessment of cloud feedback requires quantifying the spatially varying role of changes in cloud amount, altitude, and optical properties on both shortwave (SW) and longwave (LW) radiation and that even subtle changes to any of these properties can have significant effects on the planetary energy budget. Schneider (1972) performed one of the first investigations into the role of clouds as feedback mechanisms, focusing on hypothetical changes in cloud amount and altitude. His calculations showed that a negative feedback would be produced at most latitudes from an increase in low- and midlevel clouds if albedo and altitude were held fixed, but that this effect could largely be canceled by the enhanced cloud greenhouse effect caused by a rise in global mean cloud-top altitude of only a few tenths of a kilometer, a result also supported by Cess (1974, 1975). Other early studies focused on the potential increase in cloud optical depth that would occur

Corresponding author address: Mark D. Zelinka, Program for Climate Model Diagnosis and Intercomparison Lawrence Livermore National Laboratory, 7000 East Avenue, L-103, Livermore, CA 94551.
E-mail: zelinka1@llnl.gov

DOI: 10.1175/JCLI-D-11-00249.1

© 2012 American Meteorological Society

in association with global warming. Paltridge (1980), using the relationship between cloud optical depth and liquid water path derived by Stephens (1978), showed that increases in liquid water path would tend to strongly increase the amount of reflected SW radiation more than it would decrease the amount of emitted LW radiation, resulting in a large negative feedback on a warming climate. These results were reinforced in the study by Somerville and Remer (1984), who derived a large negative optical depth feedback using a 1D radiative–convective equilibrium model with empirically derived relations between temperature and cloud water content measured by aircraft over the former Soviet Union (Feigelson 1978).

Although 1D radiative–convective equilibrium models employed to quantify cloud feedback in early studies like those described above provide insight into potential cloud feedbacks, the cloud feedback operating in nature in response to external forcing is, as pointed out in Schneider et al. (1978), made up of a complex mix of time, space, and radiation-weighted cloud changes. The best chance to realistically simulate the response of clouds to external forcing is with fully three-dimensional global climate models (GCMs). Inserting global mean cloud profiles produced by the full three-dimensional Goddard Institute for Space Studies (GISS) model for a controlled and doubled-CO_2 climate into the 1D radiative convective equilibrium model of Lacis et al. (1981), Hansen et al. (1984) calculated that cloud feedback represents a significant positive feedback, made up of roughly equal contributions from decreased outgoing longwave radiation (OLR) due to increased cloud altitude and increased absorbed solar radiation due to decreased cloud amount. Wetherald and Manabe (1988) found similar patterns of cloud changes in the Geophysical Fluid Dynamics Laboratory (GFDL) model—namely, a reduction in low- and midlevel clouds and an increase in the altitude of tropical high clouds. They used the partial radiative perturbation (PRP) technique (Wetherald and Manabe 1980) to show that the LW cloud amount and altitude feedbacks tended to oppose one another, resulting in a positive LW cloud feedback that was roughly half as large as the positive SW cloud feedback.

Roeckner et al. (1987) performed the first doubled-CO_2 GCM experiments in which cloud liquid water was included prognostically, and found, after clarification by Schlesinger (1988), that increases in cloud liquid water path and optical depth brought about a positive LW optical depth feedback (due to increased high cloud emissivity) that dominated over the smaller negative SW optical depth feedback (due to increased cloud reflectivity). This result later received further support from the uniform ±2-K sea surface temperature perturbation experiments of Taylor and Ghan (1992) for the National Center for Atmospheric Research (NCAR) model, but Senior and Mitchell (1993) found that phase changes from ice to water in doubled-CO_2 experiments in the Met Office model brought about large negative SW cloud feedbacks, with contributions primarily coming from clouds at mid- and high latitudes.

Colman et al. (2001), using an earlier version of the Bureau of Meteorology Research Centre (BMRC) model, performed perhaps the most comprehensive analysis of cloud feedback due to a doubling of CO_2, separating the feedback into components due to changes in cloud amount, altitude, and optical depth, with the latter further broken down into components due to changes in total water, phase, convective cloud fraction, and in-cloud temperature (a proxy for cloud geometric thickness). Using the PRP method, they computed large negative contributions to the LW cloud feedback from reductions in cloud fraction and positive contributions from changes in cloud altitude and optical depth, the latter dominated by increases in total water content of clouds. Conversely, they computed large positive contributions to the SW cloud feedback from reductions in cloud amount and increases in cloud altitude, but large negative contributions from increases in cloud optical depth, the latter being primarily due to phase changes from ice to liquid, with a smaller contribution from increases in total water content.

Though the issue of intermodel spread tends to dominate contemporary discussions of cloud feedback, it is also important to identify, quantify, and understand which aspects are robust and if there are fundamental physical explanations for such responses in a warming climate. Common features to nearly all GCM studies of global warming due to increasing greenhouse gas concentrations, including the early studies described above as well as the current generation of climate models (cf. Fig. 10.10 in Meehl et al. (2007)), are a decrease in cloud amount equatorward of about 50°, an increase in cloud amount poleward of 50°, and an overall upward shift of clouds—features that mimic the average change in relative humidity. Another feature that is emerging as robust across the models is the large increase in cloud optical depth in the region of mixed-phase clouds (roughly between 0° and −15°C) and smaller decrease at temperatures greater than freezing (Mitchell et al. 1989; Senior and Mitchell 1993; Tselioudis et al. 1998; Colman et al. 2001; Tsushima et al. 2006).

In summary, the models predict opposing effects on LW and SW radiation from changes in a variety of cloud properties. The net cloud feedback thus represents the integrated effect on radiation from spatially varying—and in many cases, subtle—cloud amount, altitude, and

optical depth responses that individually may have large magnitudes and varying degrees of compensation. Even though most models produce similar gross changes in cloud properties, estimates of cloud feedback remain widely spread relative to other feedbacks. Indeed, as first identified by Cess et al. (1989, 1990), the variation in climate sensitivities predicted by GCMs is primarily attributable to intermodel differences in cloud feedbacks. This continues to be the case in contemporary climate models (Colman 2003; Soden and Held 2006; Ringer et al. 2006; Webb et al. 2006), and recent evidence has identified the response of marine boundary layer clouds in subsidence regimes of the subtropics as primarily responsible for the intermodel spread in cloud feedback (e.g., Bony et al. 2004; Bony and Dufresne 2005; Wyant et al. 2006; Webb et al. 2006; Soden and Vecchi 2011). As we have noted in Zelinka et al. 2012 (hereafter Part I), however, this should not be taken as evidence that other cloud responses are consistently modeled or that they make a narrow range of contributions to the feedback. Attribution of the mean and spread in cloud feedbacks to the *nature* of the cloud changes from which they arise, which is the purpose of this paper, is a necessary first step in identifying their robust and nonrobust aspects and ultimately in identifying which aspects are physically plausible and potentially realistic.

In Part I of this study, we proposed a new technique for computing cloud feedback using cloud radiative kernels along with histograms of cloud fraction partitioned into cloud-top pressure (CTP) and optical depth (τ) bins by the International Satellite Cloud Climatology Project (ISCCP) simulator (Klein and Jakob 1999; Webb et al. 2001). A highly appealing aspect of this new technique is its ability to quantify the contribution to cloud feedback from individual cloud types. However, the distinction between changes in cloud amount, altitude, and optical depth in contributing to cloud feedbacks is somewhat ambiguous. For example, we found in Part I that high-cloud changes dominate the LW cloud feedback at all latitudes. This is unsurprising considering the high sensitivity of OLR to high clouds as represented by the LW cloud radiative kernel, so even if the total cloud fraction increased but the relative proportion of each cloud type in the histogram remained unchanged, high clouds would stand out as being of primary importance. It is more interesting and illuminating to quantify the contribution to the positive LW cloud feedback of rising cloud tops relative to that of changes in total cloud amount holding the vertical and optical depth distribution fixed. Similarly, it is desirable to separate the role of changes in total cloud amount from that of a shift in the cloud optical depth distribution in contributing to both LW and SW cloud feedbacks.

In this study, rather than quantifying cloud feedbacks due to cloud changes within particular bins of the histogram (as was done in Part I), we quantify the cloud feedbacks arising from changes in the distribution of clouds within the histograms (i.e., clouds moving from one bin to another) and due to proportionate changes in total cloud amount (i.e., total cloud fraction changing but the relative amounts of each cloud type in the histogram staying fixed). We perform this partitioning in an ensemble of 11 GCMs taking part in the first phase of the Cloud Feedback Model Intercomparison Project (CFMIP1), thereby providing the first model intercomparison of the LW, SW, and net cloud amount, altitude, and optical depth feedbacks.

2. Partitioning cloud feedback through a decomposition of cloud distribution changes

In this section we present the methodology we use to decompose the change in cloud fraction into components due to the proportionate change in cloud fraction, the change in CTP, and the change in τ. Each of the three feedbacks (cloud amount, altitude, and optical depth) is solely the result of changes in that component with the other two components held fixed. To separate the effect of a change in mean cloud amount from a shift in the altitude or optical depth of clouds, we divide the cloud fraction matrix into means over pressure and optical depth and departures therefrom. We note that several variants exist to define these feedbacks from the ISCCP simulator output; we have chosen the simplest and most direct method for our work, but we have seen little sensitivity to the method chosen. We will explain our methodology with the help of a 2×3 example matrix in which columns represent three τ bins and rows correspond to two CTP bins. The technique described below is applied in an analogous way to the full 7×7 matrix of the ISCCP simulator output. In our example, the CTP-τ matrix of the joint histogram of cloud fraction (expressed in percent) for a single location and month for the current climate is given by

$$\mathbf{C} = \begin{pmatrix} 2 & 3 & 1 \\ 6 & 4 & 0 \end{pmatrix},$$

and an example matrix containing the change in cloud fraction $\Delta\mathbf{C}$ between the current and $2 \times CO_2$ climate for this location and month is given by

$$\Delta\mathbf{C} = \begin{pmatrix} -1 & 0 & 2 \\ 0 & 2 & 4 \end{pmatrix}.$$

We define the total cloud fraction (C_{tot}) as

$$C_{\text{tot}} = \sum_{p=1}^{P}\sum_{\tau=1}^{T} C, \tag{1}$$

and the total change in cloud fraction (ΔC_{tot}) as

$$\Delta C_{\text{tot}} = \sum_{p=1}^{P}\sum_{\tau=1}^{T} \Delta C, \tag{2}$$

where P and T are the number of CTP and τ bins in the histogram (in this example, 2 and 3, respectively).

The hypothetical change in cloud fraction, assuming the change in total cloud fraction is distributed throughout the histogram, such that the relative proportions of cloud fractions in each CTP-τ bin remains constant, is computed as

$$\Delta\mathbf{C}_{\text{prop}} = \left(\frac{\Delta C_{\text{tot}}}{C_{\text{tot}}}\right) \times \mathbf{C}. \tag{3}$$

The first term in Eq. (3) is a scalar representing the fractional change in total cloud fraction. This decomposition isolates the contribution of changes in total cloud fraction from changes in the vertical and optical depth distribution of clouds. Using the example values,

$$\Delta\mathbf{C}_{\text{prop}} = \frac{7}{16} \times \begin{pmatrix} 2 & 3 & 1 \\ 6 & 4 & 0 \end{pmatrix} = \begin{pmatrix} 0.88 & 1.31 & 0.44 \\ 2.63 & 1.75 & 0.00 \end{pmatrix}.$$

The sum of the $\Delta\mathbf{C}_{\text{prop}}$ histogram is exactly equal to the change in total cloud fraction, but the histogram is constructed in such a way that the relative proportion of clouds in each bin remains constant. We will refer to $\Delta\mathbf{C}_{\text{prop}}$ as the proportionate change in cloud fraction. To compute the cloud feedback associated it, which we refer to as the cloud amount feedback, we multiply this matrix by the corresponding entries of the cloud radiative kernel for its location and month.

To compute the cloud altitude feedback, we first compute the hypothetical change in the distribution of cloud fractions, assuming the total cloud fraction remains constant and the relative proportion of cloud fraction in each τ bin (column) remains constant. This is computed by performing the following subtraction at each pressure bin (row):

$$\Delta\mathbf{C}_{\Delta p} = \Delta\mathbf{C} - \frac{1}{P}\sum_{p=1}^{P} \Delta\mathbf{C}. \tag{4}$$

This computation takes the anomalous cloud fraction histogram and subtracts from each τ bin (column) the mean anomaly across all CTP bins (rows). This decomposition isolates the contribution of changes in the vertical distribution of clouds from the changes in total cloud fraction and changes in the optical depth distribution of clouds. Using the example values,

$$\Delta\mathbf{C}_{\Delta p} = \begin{pmatrix} -1 & 0 & 2 \\ 0 & 2 & 4 \end{pmatrix} - \begin{pmatrix} -0.50 & 1.00 & 3.00 \\ -0.50 & 1.00 & 3.00 \end{pmatrix} = \begin{pmatrix} -0.50 & -1.00 & -1.00 \\ 0.50 & 1.00 & 1.00 \end{pmatrix}.$$

Note that, by definition, $\sum_{p=1}^{P}\Delta\mathbf{C}_{\Delta p} = 0$ for all τ bins and $\sum_{p=1}^{P}\sum_{\tau=1}^{T}\Delta\mathbf{C}_{\Delta p} = 0$. In other words, $\mathbf{C}$ and $\mathbf{C} + \Delta\mathbf{C}_{\Delta p}$ have the same total amount of cloud and relative proportion of clouds in each τ bin. Multiplying $\Delta\mathbf{C}_{\Delta p}$ by the corresponding cloud radiative kernel for each location and month yields the cloud altitude feedback.

In a similar manner, to determine the cloud optical depth feedback, we compute the hypothetical change in the distribution of cloud fractions, assuming the total cloud fraction as well as the relative proportion of clouds in each CTP bin (row) remains constant. This is computed by performing the following subtraction at each τ bin (column):

$$\Delta\mathbf{C}_{\Delta\tau} = \Delta\mathbf{C} - \frac{1}{T}\sum_{\tau=1}^{T} \Delta\mathbf{C}. \tag{5}$$

This computation takes the anomalous cloud fraction histogram and subtracts from each CTP bin (row) the mean anomaly across all τ bins (columns). This decomposition isolates the contribution of changes in the optical depth distribution of clouds from the changes in total cloud fraction and changes in the vertical distribution of clouds. Using the example values,

$$\Delta\mathbf{C}_{\Delta\tau} = \begin{pmatrix} -1 & 0 & 2 \\ 0 & 2 & 4 \end{pmatrix} - \begin{pmatrix} 0.33 & 0.33 & 0.33 \\ 2.00 & 2.00 & 2.00 \end{pmatrix} = \begin{pmatrix} -1.33 & -0.33 & 1.67 \\ -2.00 & 0.00 & 2.00 \end{pmatrix}.$$

Note that, by definition, $\sum_{\tau=1}^{T}\Delta\mathbf{C}_{\Delta\tau} = 0$ for all CTP bins and $\sum_{p=1}^{P}\sum_{\tau=1}^{T}\Delta\mathbf{C}_{\Delta\tau} = 0$. In other words, $\mathbf{C}$ and $\mathbf{C} + \Delta\mathbf{C}_{\Delta\tau}$ have the same total amount of cloud and relative proportion of clouds in each CTP bin. Multiplying $\Delta\mathbf{C}_{\Delta\tau}$ by the cloud radiative kernel yields the cloud optical depth feedback.

The sum of the three decomposed matrices should roughly reproduce the true $\Delta\mathbf{C}$ matrix but, in general, residuals remain in one or more bins. These residuals arise from coincident changes in, for example, cloud altitude

and cloud optical depth, that do not unambiguously fall into one of our categories of decomposition. Summing $\Delta\mathbf{C}_{\text{prop}}$, $\Delta\mathbf{C}_{\Delta p}$, and $\Delta\mathbf{C}_{\Delta\tau}$ gives

$$\begin{pmatrix} -0.96 & -0.02 & 1.10 \\ 1.13 & 2.75 & 3.00 \end{pmatrix}.$$

Note that the sum of this matrix is constrained to exactly equal the true change in cloud fraction (7 in this example). The residual is

$$\Delta\mathbf{C}_{\text{residual}} = \begin{pmatrix} -1 & 0 & 2 \\ 0 & 2 & 4 \end{pmatrix} - \begin{pmatrix} -0.96 & -0.02 & 1.10 \\ 1.13 & 2.75 & 3.00 \end{pmatrix} = \begin{pmatrix} -0.04 & 0.02 & 0.90 \\ -1.13 & -0.75 & 1.00 \end{pmatrix}.$$

The residual matrix sums to zero by design, but it does contribute to the cloud feedback calculation because it is multiplied with the cloud radiative kernel before being summed. As shown below, this is generally a small contribution because the first-order components of the feedback are accounted for by the effect of cloud amount, altitude, and optical depth changes.

Before continuing, it is important to recognize that aliasing can arise from partitioning cloud feedback using this decomposition. This is because the decomposed cloud fraction anomaly joint histograms may have nonzero elements even where cloud fraction anomalies are zero. A particularly egregious example would be a hypothetical large reduction in low, thin cloud fraction, with no change in the fraction of any other cloud type. This would appear in our altitude decomposition as both a negative low cloud anomaly and a positive cloud anomaly at other altitudes within the thin τ bin, and in our optical depth decomposition as both a negative thin cloud anomaly and a positive cloud anomaly at other optical thicknesses within the low CTP bin. The proportionate change in cloud fraction histogram will have negative values in every element for which the mean state cloud fraction histogram is nonzero. In other words, the effect of a change in the fraction of an individual cloud type may (i) be included in more than one decomposition and (ii) get ''spread'' among the other elements of the decomposed histograms. When multiplied by the cloud radiative kernels, this could produce appreciable cloud amount, altitude, and/or optical depth feedbacks, even though the radiative impact of that individual cloud fraction anomaly is small. Locations in which the sum of amount, altitude, and optical depth feedbacks are affected by such ''spreading'' will have nonzero residual feedbacks. Thus, care must be taken when interpreting the magnitude of the amount, altitude, and optical depth feedbacks, especially where the residual term is of comparable magnitude.

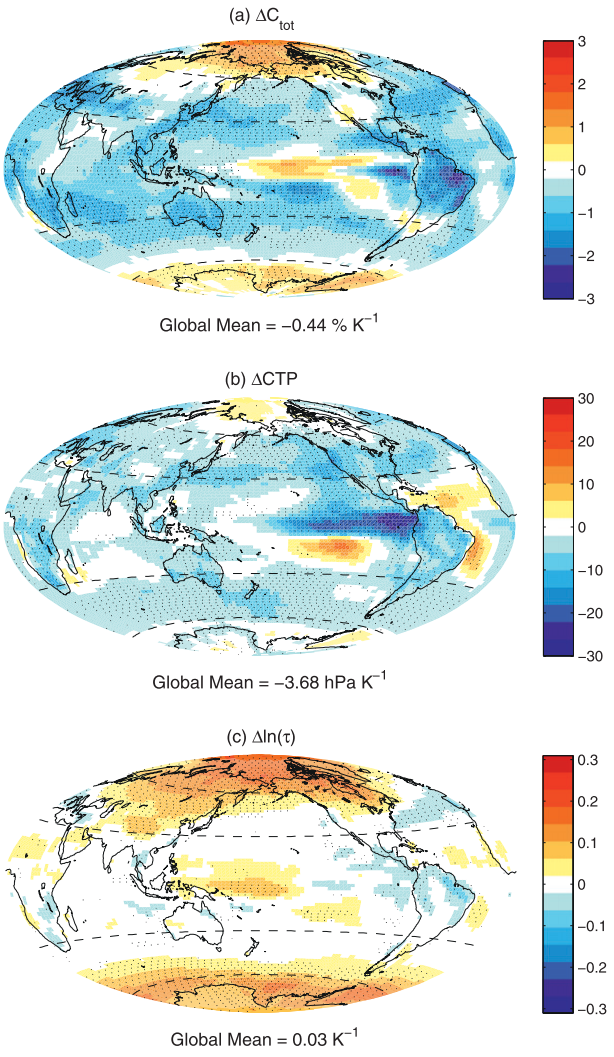


FIG. 1. Annual and ensemble mean change in (a) cloud fraction, (b) cloud fraction–weighted cloud-top pressure, and (c) cloud fraction–weighted natural logarithm of optical depth per degree global average surface air temperature increase. Stippling indicates regions where ≥75% of the models agree on the sign of the field plotted. The dashed lines are the ±30° and ±60° latitude lines.

3. Ensemble mean change in cloud properties

As an aid in interpreting the contributions to cloud feedbacks from the three types of cloud changes decomposed above, in Fig. 1 we show the ensemble mean change in total cloud fraction, CTP, and the natural logarithm of τ per degree of global average surface air temperature warming. The change in $\ln(\tau)$ rather than in τ is calculated because the former quantity is linearly proportional to the

change in albedo (e.g., Twomey 1977). The latter two quantities are computed by differencing the cloud fraction–weighted mean of the midpoints of each CTP or $\ln(\tau)$ bin between the control and doubled-CO_2 climate. For simplicity, we will refer to these as changes in CTP and $\ln(\tau)$ rather than as changes in cloud fraction–weighted CTP and cloud fraction–weighted $\ln(\tau)$. Henceforth, the ensemble refers to all the models except the Max Planck Institute ECHAM5 (mpi_echam5) model, which is excluded based on discrepancies discussed in Part I. Stippling indicates where $\geq$75% of the models (i.e., 9 out of 11) agree on the sign of the field plotted, and we will hereafter refer to features with this level of agreement among the models as ''robust.'' Unless otherwise noted, all results in this paper are for annual mean quantities.

Cloud fraction decreases nearly everywhere between 55°S and 60°N and increases nearly everywhere poleward of these latitudes (Fig. 1a). An exception to this pattern is a large region of increased cloud fraction in the central equatorial Pacific, which results from an eastward shift in convection tracking higher SSTs, though this is not a robust feature. Cloud fraction reductions are prominent in the subtropics, especially over the continents. Large increases in cloud fraction tend to occur where regions formerly covered with sea ice become open water in the warmed climate. The general pattern of a decrease in cloud fraction equatorward of 50° is consistent with many previous studies (e.g., Wetherald and Manabe 1988; Senior and Mitchell 1993; Colman et al. 2001; Meehl et al. 2007).

Changes in CTP (Fig. 1b) are negative nearly everywhere except in regions that become dominated by low cloud types (e.g., in the Arctic and in the central Pacific just south of the equator), though the positive CTP changes are generally not robust. Note that these values represent the change in cloud fraction–weighted CTP; thus, a location in which the cloud regime changes between the two climates (e.g., if the location switches from being a low cloud–dominated regime to a high cloud–dominated one) will exhibit large changes in this quantity. Therefore, one must interpret the values on this map as representing some combination of vertical shifts in the cloud types present and changes in the frequency of occurrence of lower cloud regimes relative to higher cloud regimes. Nevertheless, the tendency for tropical clouds to systematically rise as the planet warms is consistent with theory [i.e., the fixed anvil temperature hypothesis of Hartmann and Larson (2002)], cloud-resolving model experiments (Tompkins and Craig 1999; Kuang and Hartmann 2007; Harrop and Hartmann 2012), other ensembles of GCM experiments (Zelinka and Hartmann 2010), and observations of warming associated with El Niño (Zelinka and Hartmann 2011). In the extratropics, rising clouds are also consistent with a rising tropopause from a warmer troposphere and colder stratosphere due to CO_2 (Kushner et al. 2001; Santer et al. 2003; Lorenz and DeWeaver 2007).

The map of changes in $\ln(\tau)$ exhibits a remarkable structure characterized by large, robust increases in $\ln(\tau)$ at latitudes poleward of about 40° and generally smaller, less-robust decreases at low latitudes (Fig. 1c). Increases in $\ln(\tau)$ associated with global warming extend farther equatorward over the continents and exhibit a large seasonal cycle (not shown) apparently driven by the larger seasonal variation in temperature relative to the oceans. As in the case of changes in CTP, it is important to keep in mind that the change in $\ln(\tau)$ does not distinguish between changes in the relative proportion of lower versus higher optical depth regimes and changes in optical thickness of a given cloud type. The modeled optical depth changes are qualitatively consistent with relationships derived from ISCCP observations, in which optical thickness increases with temperature for cold low clouds but decreases with temperature for warm low clouds (Tselioudis et al. 1992; Tselioudis and Rossow 1994).

The high-latitude cloud optical thickness response is likely related to changes in the phase and/or total water contents of clouds that lead to increases in optical thickness as temperature increases. As evidence, the fractional changes, per degree of global warming, in total, ice, and liquid water paths are shown in Fig. 2. The latter quantity is computed from the difference in the former two quantities. Because of limitations in the archive of CFMIP1 cloud output, we cannot unambiguously separate these changes in gridbox mean water path into their contributions from changes in cloud amount or in-cloud water paths. Nevertheless, large, robust increases in total water path occur at high latitudes (Fig. 2a), and are clearly dominated by the liquid phase (Fig. 2c).

Several lines of evidence suggest that the increase in high-latitude cloud water content is realistic and that such changes should result in clouds becoming more optically thick. In observations, the total water contents of liquid and ice clouds tend to increase with temperature (Feigelson 1978; Somerville and Remer 1984; Mace et al. 2001) at rates approaching that of the increase in adiabatic water content (i.e., the amount of water condensed into a parcel that is ascending moist adiabatically within a cloud) with temperature. Betts and Harshvardan (1987) demonstrated analytically that this rate is twice as large at high latitudes than at low latitudes. Additionally, a higher freezing level associated with a warmer atmosphere promotes more liquid-phase clouds, which—because of the Bergeron–Findeisen effect—tend to precipitate less

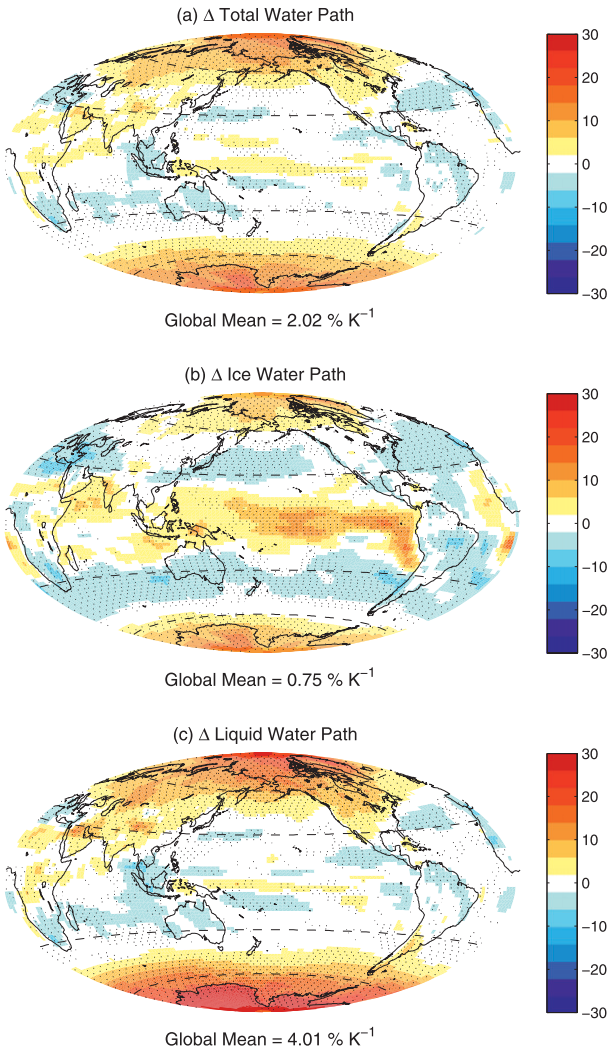


FIG. 2. Annual and ensemble mean percentage change in (a) total water path, (b) ice water path, and (c) liquid water path per degree global average surface air temperature increase. Stippling indicates regions where ≥75% of the models agree on the sign of the field plotted. The BMRC1; IPSL_CM4; and Model for Interdisciplinary Research on Climate 3.2, high-resolution version [MIROC3.2(hires)] models are excluded because they did not archive total water path or ice water path.

efficiently and have larger water contents than ice- or mixed-phase clouds (Senior and Mitchell 1993; Tsushima et al. 2006). Finally, even if total water content were to remain constant, the smaller size of liquid droplets relative to ice crystals tends to enhance cloud reflectivity and therefore increase optical depth.

4. Ensemble mean cloud feedback contributions

Decomposed contributions to the ensemble mean LW cloud feedback are shown in Fig. 3. Increasing cloud-top altitude is the dominant contributor to the LW cloud feedback, providing 0.39 W m^{-2} K^{-1} in the global mean (Fig. 3c). As in Zelinka and Hartmann (2010), we find that the ensemble mean contribution of rising *tropical* clouds to the LW cloud feedback (0.44 W m^{-2} K^{-1}) is roughly twice as large as the global mean LW cloud feedback (0.21 W m^{-2} K^{-1}). Because the tropics represents half the area of the planet, this means that the LW cloud amount, optical depth, residual, and extratropical altitude feedbacks cancel in the global mean, and that the global mean feedback is simply equal to the contribution from the tropical LW cloud altitude feedback. This result is not robust across the models, however. A noteworthy feature of the ensemble mean is that the 0.34 W m^{-2} K^{-1} contribution of rising cloud tops to the LW cloud feedback in the extratropics (latitude $> 30°$) is only 25% smaller than that in the tropics. These results confirm the importance of rising cloud tops to the positive LW cloud feedback, but the −0.29 W m^{-2} K^{-1} global mean contribution from reductions in cloud amount (Fig. 3b) offsets 75% of the altitude effect. We are aware of no fundamental reasons to expect the upward shift to dominate over cloud fraction reductions in bringing about a positive LW cloud feedback; indeed, in some models, the latter effect is larger (as discussed in the section 5).

The contribution of changes in cloud optical depth is smaller in the global mean than that due to changes in cloud amount and altitude, but it is nonetheless positive nearly everywhere (Fig. 3d). Notably, robust optical depth increases are the primary positive contribution to LW cloud feedback poleward of about 60° in both hemispheres, strongly opposing the locally negative altitude feedback over the polar oceans. In the global mean, the positive contribution to LW cloud feedback from optical depth increases is roughly half as large as that from cloud altitude increases.

Finally, the LW cloud feedback arising from residuals in the change in cloud fraction decomposition (Fig. 3e) is negative everywhere except at very high latitudes. Its magnitude is largest where both the LW altitude and optical depth feedbacks are positive, indicating that the decomposition incorporates some cloud anomalies into both the altitude and optical depth feedbacks, causing a slight overestimate of their combined LW impact.

Decomposed contributions to the ensemble mean SW cloud feedback are shown in Fig. 4. The dominant contributor to the SW cloud feedback at most locations and in the global mean is the change in cloud fraction holding the vertical and optical depth distribution fixed (Fig. 4b). With the exception of the equatorial Pacific, where nonrobust increases in cloud fraction occur in the ensemble mean, robust reductions in cloud fraction at

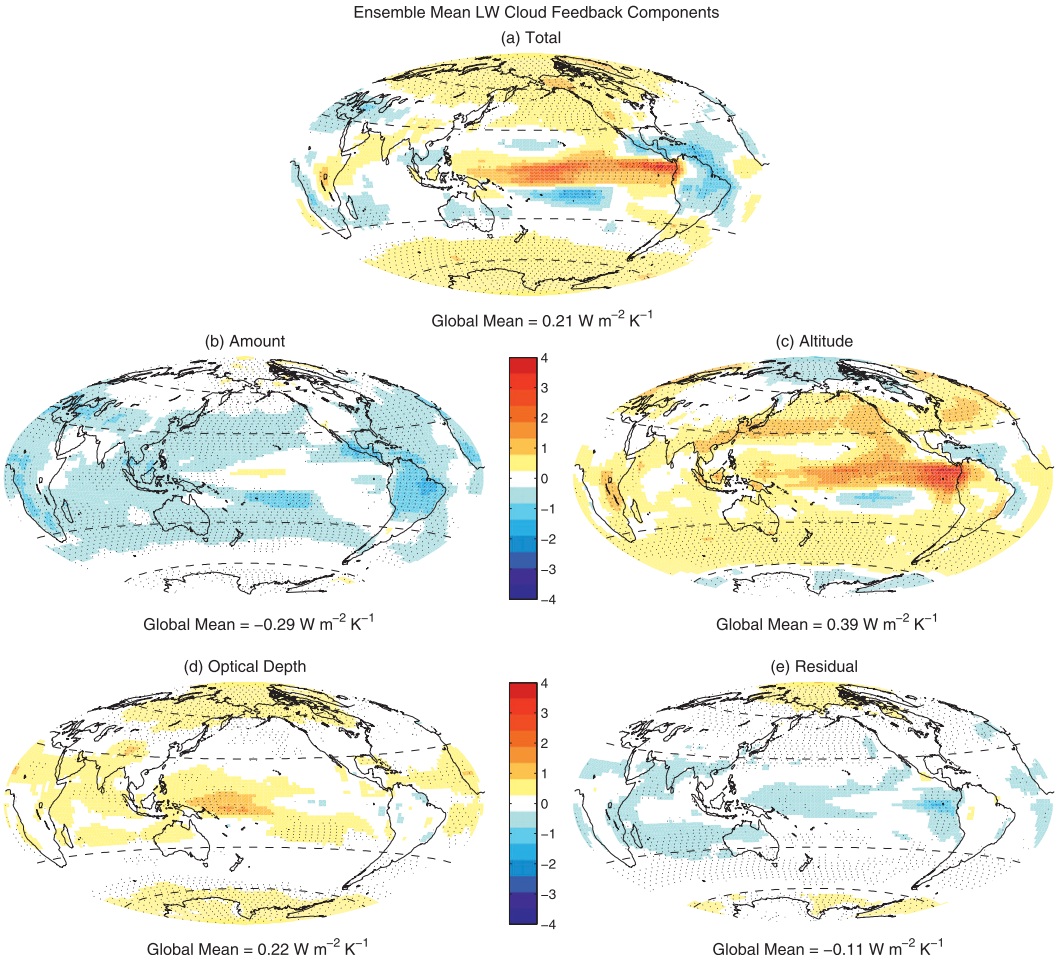


FIG. 3. Annual and ensemble mean (a) LW cloud feedback and components due to the (b) proportionate change in cloud fraction, (c) change in cloud vertical distribution, (d) change in cloud optical depth distribution, and (e) residual term. Stippling indicates regions where ≥75% of the models agree on the sign of the field plotted.

most locations between 50°S and 65°N contribute to a positive SW cloud feedback.

Although cloud-top altitude robustly increases, its impact on SW fluxes is negligible everywhere (Fig. 4c). The global average SW cloud altitude feedback is slightly negative, however, owing to the slight increase in SW flux sensitivity to cloud fraction changes with decreasing cloud-top pressure (cf. Fig. 1b in Part I).

In the global mean, the SW optical depth feedback is negative and considerably smaller in magnitude than the SW cloud amount feedback, but it is regionally very important (Fig. 4d). Equatorward of about 40° but excluding the tropical western Pacific (where high clouds become thicker), the SW optical depth feedback is positive due to decreases in τ of low- and midlevel clouds. Consistent with this, Tselioudis et al. (1992), Tselioudis and Rossow (1994), and Chang and Coakley (2007) have shown using satellite observations that low- and midlatitude boundary layer clouds experience a decrease in optical depth as temperature increases. The most dramatic and robust feature of the optical depth feedback is the presence of large negative values at high latitudes in either hemisphere, which locally dominate the other contributions to SW cloud feedback. As discussed in the previous section, several lines of evidence suggest that cold clouds are particularly susceptible to increases in temperature that act to increase their optical depth, providing a possible physical basis for the modeled increases in τ (Fig. 1c) and for the subsequent large negative optical depth feedback at high latitudes shown here.

In Fig. 5 we show the decomposed contributions to the ensemble mean net cloud feedback, which is quite strongly positive (0.57 W m^{-2} K^{-1}). Proportionate changes in cloud fraction (Fig. 5b) contribute 0.27 W m^{-2} K^{-1} to the net cloud feedback, while rising cloud tops (Fig. 5c)

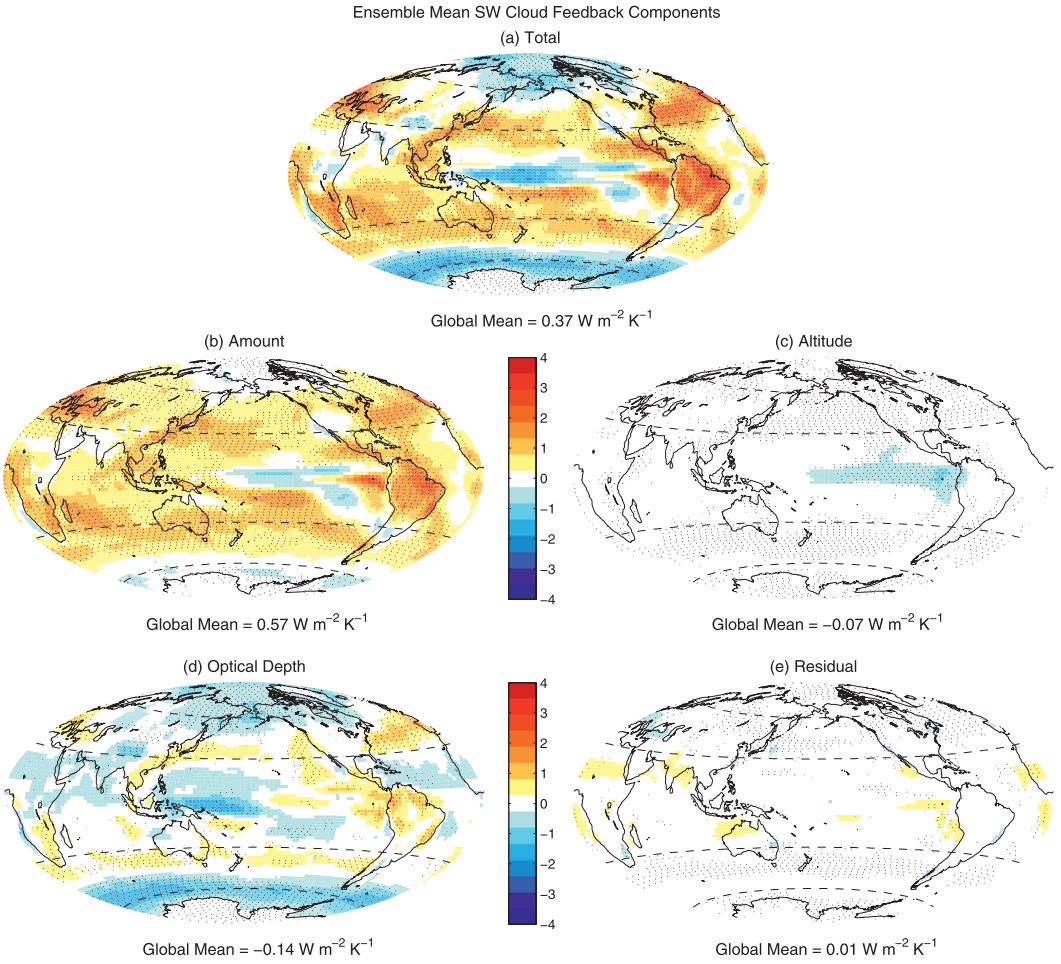


FIG. 4. As in Fig. 3, but for the SW cloud feedback partitioning.

contribute 0.33 W m^{-2} K^{-1}. That the contribution of rising cloud tops is slightly larger than the contribution of decreasing cloud amount is an important result because one could argue that fundamental constraints exist on cloud altitude and its changes, namely, the location of radiatively driven divergence in the tropics (Hartmann and Larson 2002; Zelinka and Hartmann 2010), and the height of the tropopause in the extratropics (Kushner et al. 2001; Santer et al. 2003; Lorenz and DeWeaver 2007). This means that a significant portion of the ensemble mean net cloud feedback arises from relatively well-understood physical processes that are robust, not particularly sensitive to assumptions made in model parameterizations, and demonstrably positive.

The contribution of optical depth changes, though small in the global mean (0.07 W m^{-2} K^{-1}), is the primary cause of the large negative values of net cloud feedback over the Arctic and Southern Ocean (Fig. 5d). Although the global mean optical depth feedback is greater in the LW than in the SW, the net optical depth feedback map more closely resembles the SW optical depth feedback map. This is because the global mean LW optical depth feedback is the average of generally small but almost systematically positive values, whereas the global mean SW optical depth feedback is made up of locally large values that partially offset each other when averaged across different regions. These features arise because LW fluxes are only sensitive to emissivity changes of higher clouds, whereas SW fluxes are sensitive to optical depth changes at all altitudes, and warm (cold) clouds tend to become less (more) optically thick as the planet warms (e.g., Tsushima et al. 2006).

Similar to its structure in the LW, the net cloud feedback arising from residuals in the change in cloud fraction decomposition (Fig. 5e) is small and negative almost everywhere except at very high latitudes, with a global mean value of −0.10 W m^{-2} K^{-1}. Its magnitude is generally large where the net amount, altitude, and optical depth feedbacks share the same sign, indicating

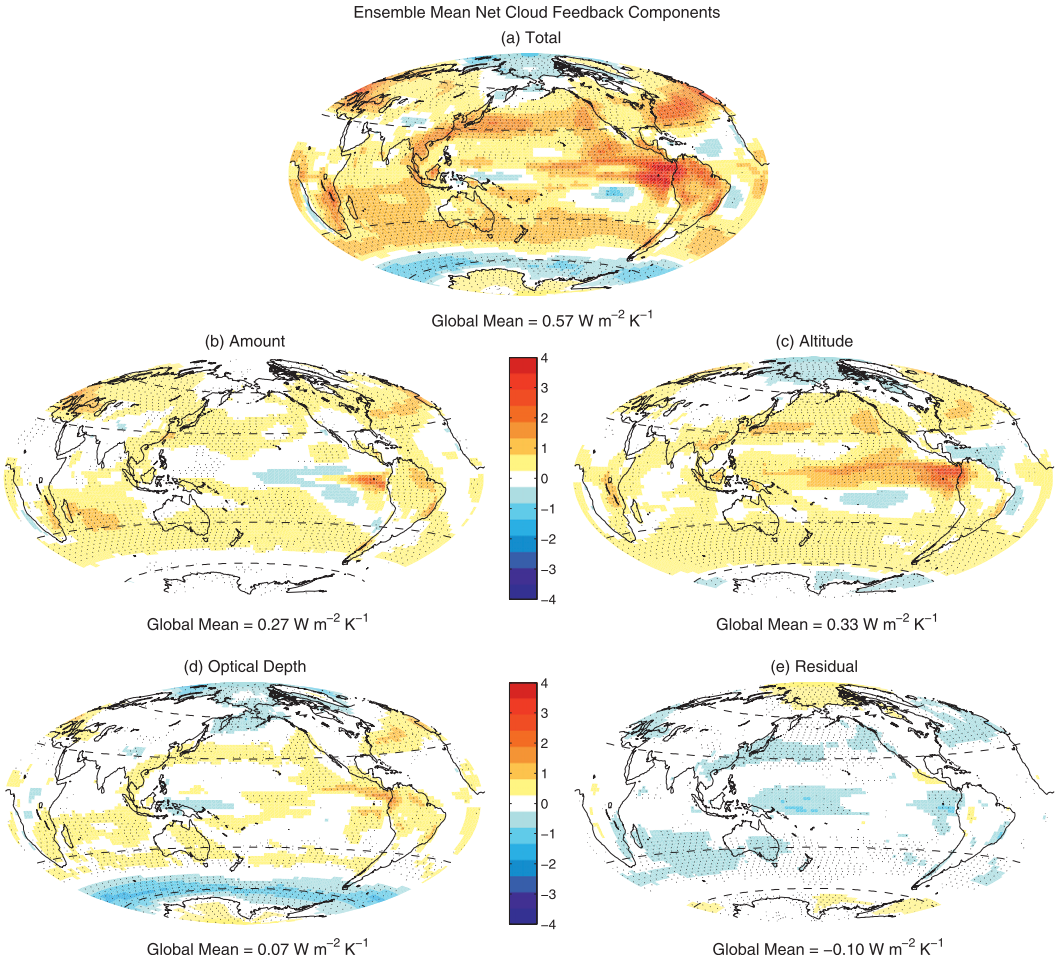


FIG. 5. As in Fig. 3, but for the net cloud feedback partitioning.

that the decomposition incorporates some cloud anomalies into all three primary feedbacks, causing a slight overestimate of their combined impact on LW + SW fluxes.

Whereas the effect of cloud amount changes on the net cloud feedback is dominated by the SW contribution (i.e., Fig. 5b looks like Fig. 4b), the effect of changes in the vertical distribution of clouds on the net cloud feedback is entirely due to the LW contribution (i.e., Fig. 5c looks like Fig. 3c). Large positive contributions from both the reduction in total cloud fraction and the upward shift of clouds produces the generally positive and robust net cloud feedback between 50°S and 65°N. The large robust negative contribution from the increase in cloud optical thickness produces the large negative cloud feedback over the Arctic and Southern Ocean.

That the cloud optical depth feedback dominates over the cloud amount feedback at high latitudes is a surprising result, considering that the large locally negative cloud feedback is often attributed (e.g., Weaver 2003; Vavrus et al. 2009; Wu et al. 2011) to cloud fraction increases associated with the poleward-shifted storm track (Hall et al. 1994, Yin 2005). Recently, Trenberth and Fasullo (2010) asserted that unrealistically small cloud fractions in the mean state of the CMIP3 models permit unrealistically large cloud fraction increases and negative cloud feedbacks over the Southern Ocean as the planet warms. Indeed, we find that appreciable robust cloud fraction increases do occur at high latitudes (Fig. 1a), and that these do contribute slightly to the negative cloud feedback there (Fig. 4b). However, here we show that it is not the increase in cloud fraction but rather the shift toward brighter clouds that primarily causes this large local negative cloud feedback. If cloud optical depth rather than cloud amount is biased low, then it is quite possible that models produce unrealistic increases in cloud brightness as the planet warms, because albedo is more sensitive to τ changes at low values of τ. Conversely, if cloud optical depth is biased high, as has been shown in several studies (e.g., Lin and Zhang 2004;

Zhang et al. 2005), then the local negative SW optical depth feedback is in fact *underestimated* compared to a model with more realistic mean state optical depths, as discussed in Bony et al. (2006). In light of this and the physical mechanisms discussed above, we consider the negative cloud feedback in the 50°–60°S latitude band to be plausible.

One must keep in mind, however, that the optical depth feedback as we have defined it does not distinguish a change in optical depth due to morphological changes in cloud type (e.g., from thin boundary layer clouds to thicker frontal clouds) that may be associated with a storm-track shift from a change in optical depth due to a change in optical properties of the cloud types that are already present (e.g., thin boundary layer clouds becoming thicker). If the former is true, then the negative high-latitude cloud feedback may indeed be caused by the poleward shift of the storm track, but manifested in the increase in mean optical depth rather than in cloud amount. If the latter is true, then this feedback arises from purely thermodynamic processes that lead to increased cloud liquid water content. Most likely some combination of both processes contributes to this feedback, but Figs. ESM 10, 14 in Williams and Webb (2009) suggest that the latter process dominates.

To more completely illuminate the cloud changes that result in a change from positive to negative cloud feedback with latitude over the Southern Ocean, we show the mean cloud fraction histograms in the control and doubled-CO_2 climates, their difference, and the corresponding feedbacks for the 30°–50°S region in Fig. 6 and for the 50°–70°S region in Fig. 7. In both regions, the mean cloud fraction histogram primarily exhibits features of the stratocumulus, frontal, and cirrus regimes identified by Williams and Webb (2009), though clouds in the 50°–70°S region tend to be thinner and lower than those in the 30°–50°S region. The total cloud fraction is roughly 15% (absolute) larger at 50°–70°S. The change in cloud fraction histogram that occurs due to climate change is remarkably different between these two regions (Figs. 6c, 7c), indicating that clouds are not simply moving from the 30°–50°S region to the 50°–70°S region. At 30°–50°S, the anomalous cloud fraction histogram exhibits a robust reduction in cloudiness at low levels and a robust increase in the altitude of high clouds, features that strongly resemble the global mean ΔC (cf. Fig. 2c in Part I). In contrast, at 50°–70°S, the primary change is a robust increase in cloudiness at large optical depths at all altitudes and decreases in the amount of low optical depth clouds, with an overall small increase in total cloudiness.

In the 30°–50°S region, increased cloudiness at the highest levels contributes to a small LW cloud feedback, but the resultant large positive net cloud feedback is primarily caused by reduced SW reflection from large reductions in cloud fraction at low and midlevels. In contrast, at 50°–70°S, the shift toward thicker clouds gives rise to a large positive LW cloud feedback and negative SW cloud feedback. The effects of thickening high clouds on LW and SW fluxes largely offset each other, and the net cloud feedback is dominated by the large shift toward thicker clouds at the lowest levels, making it moderately negative.

The changes in cloud distribution that occur in these regions likely reflect some combination of changes in the relative proportion of cloud types (stratocumulus, frontal, etc.) and changes in the properties of the individual cloud types, as shown in Williams and Webb (2009). A striking feature that is apparent from comparing Fig. 6a with Fig. 6b and Fig. 7a with Fig. 7b, however, is the subtle nature of the changes that occur to the cloud fraction histograms in going from a control to a perturbed climate. That such nearly visually indiscernible changes in cloud distribution between the perturbed and control climates can produce large radiative fluxes is rather humbling, in that it underscores an acute challenge of constraining cloud feedbacks.

The zonal and ensemble mean cloud feedbacks and their partitioning among the three components described above are shown in Fig. 8. The robust but competing effects of rising cloud tops and decreasing cloud coverage on the LW cloud feedback are apparent at most latitudes, with the LW cloud altitude feedback dominating at most latitudes, especially in the deep tropics and midlatitudes. Proportionate cloud amount changes are the dominant contributor to the SW cloud feedback at nearly every latitude except at high latitudes, where the large increase in optical depth dominates. The relative dominance of each contributor to the net cloud feedback varies as a function of latitude, but all components are generally positive except at high latitudes, where the optical depth feedback is large and negative. In general, the net residual contribution opposes the other components, most strongly where all three components have the same sign.

Several features of the feedbacks shown in Fig. 8 nicely synthesize the results shown in Figs. 6, 7 in Part I. For instance, it is apparent that the increase of high clouds at the expense of midlevel clouds (Fig. 6a in Part I) strongly contributes to the extratropical maxima in the LW altitude feedback (Fig. 8a). Also, regions in which thick clouds increase at the expense of medium-thickness clouds (most prominently at latitudes greater than 50° but also in the deep tropics, as shown in Fig. 7b in Part I) are clearly the regions in which the optical depth feedback is negative (Fig. 8b). Thus, the decomposition performed

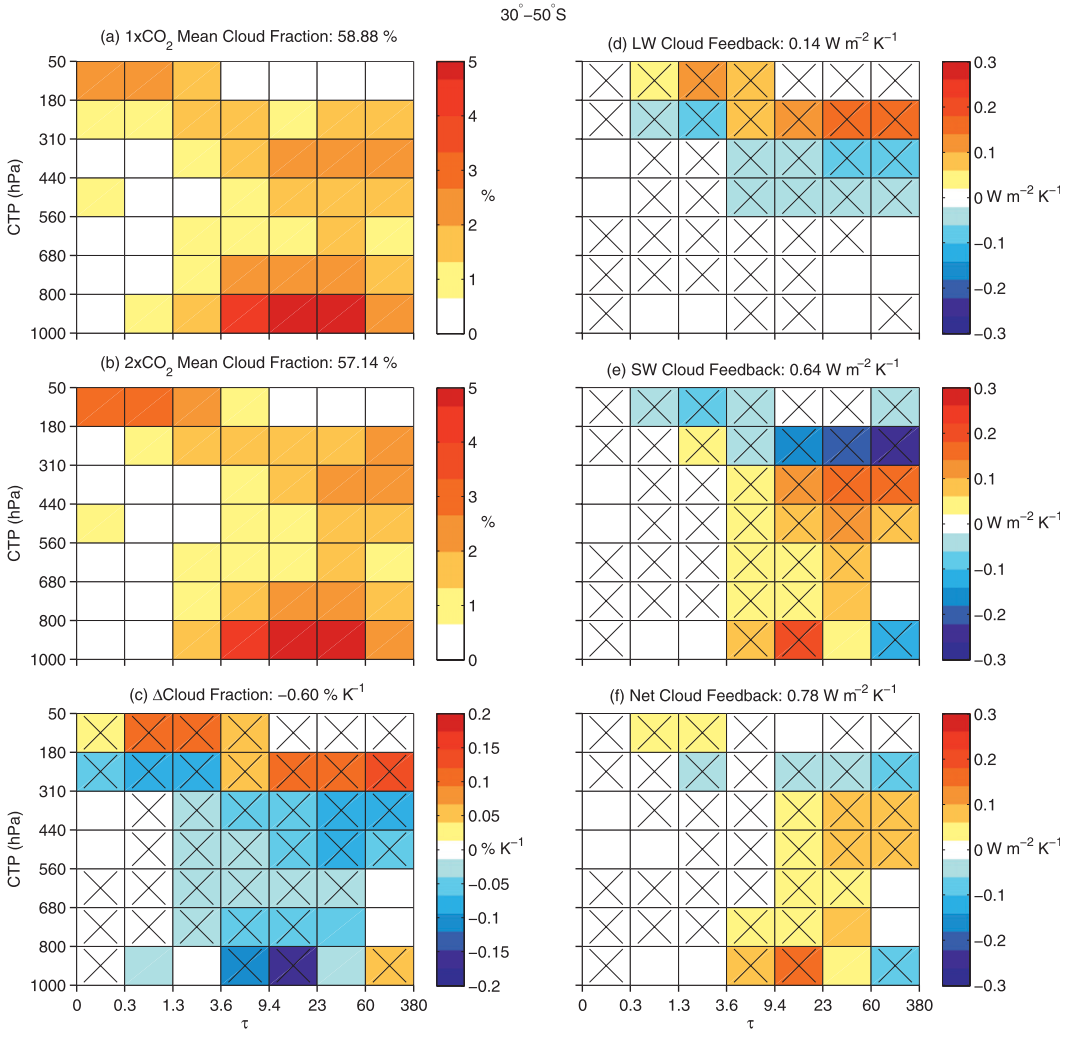


FIG. 6. Annual and ensemble mean cloud fraction in the 30°–50°S region for the (a) 1 × CO_2 and (b) 2 × CO_2 runs, along with (c) the difference expressed per unit change in each model's global mean surface air temperature between the two states. Matrix resulting from multiplying the change in cloud fraction at each month and location in the 30°–50°S region with the collocated (d) LW, (e) SW, and (f) net cloud radiative kernels, then taking the spatial, annual, and ensemble mean. The sum of each matrix is shown in each title. Bins containing an "X" indicate those in which ≥75% of the models agree on the sign of the field plotted.

here provides a clear way of synthesizing the gross impact of cloud changes that may be difficult to discern from assessing the impact of individual cloud types, which can exhibit significant compensation.

5. Intermodel spread in cloud feedback contributions

In Figs. 9, 10 we show global mean cloud feedback estimates and their partitioning among cloud amount, altitude, optical depth, and residual components for each model and for the multimodel mean. The bar plots in Fig. 9 allow for assessment of the combination of cloud responses that give rise to the global mean LW, SW, and net cloud feedbacks in each model. Figure 10 displays these results in a more compact manner, facilitating a visual comparison of the mean and spread in individual feedback components and determination of robust and nonrobust feedback components.

The LW cloud feedback estimates span a range of 0.82 from −0.13 to 0.69 W m^{-2} K^{-1}, though only the BMRC1 model has a negative value. (Note that neither of the two tests for proper simulator implementation discussed in Part I could be performed for the BMRC1 model.) In every model, proportionate reductions in global mean cloud fraction act to reduce the LW cloud feedback, with values spanning a range of 0.58 from −0.63 to −0.05 W m^{-2} K^{-1}. The dominant contributor

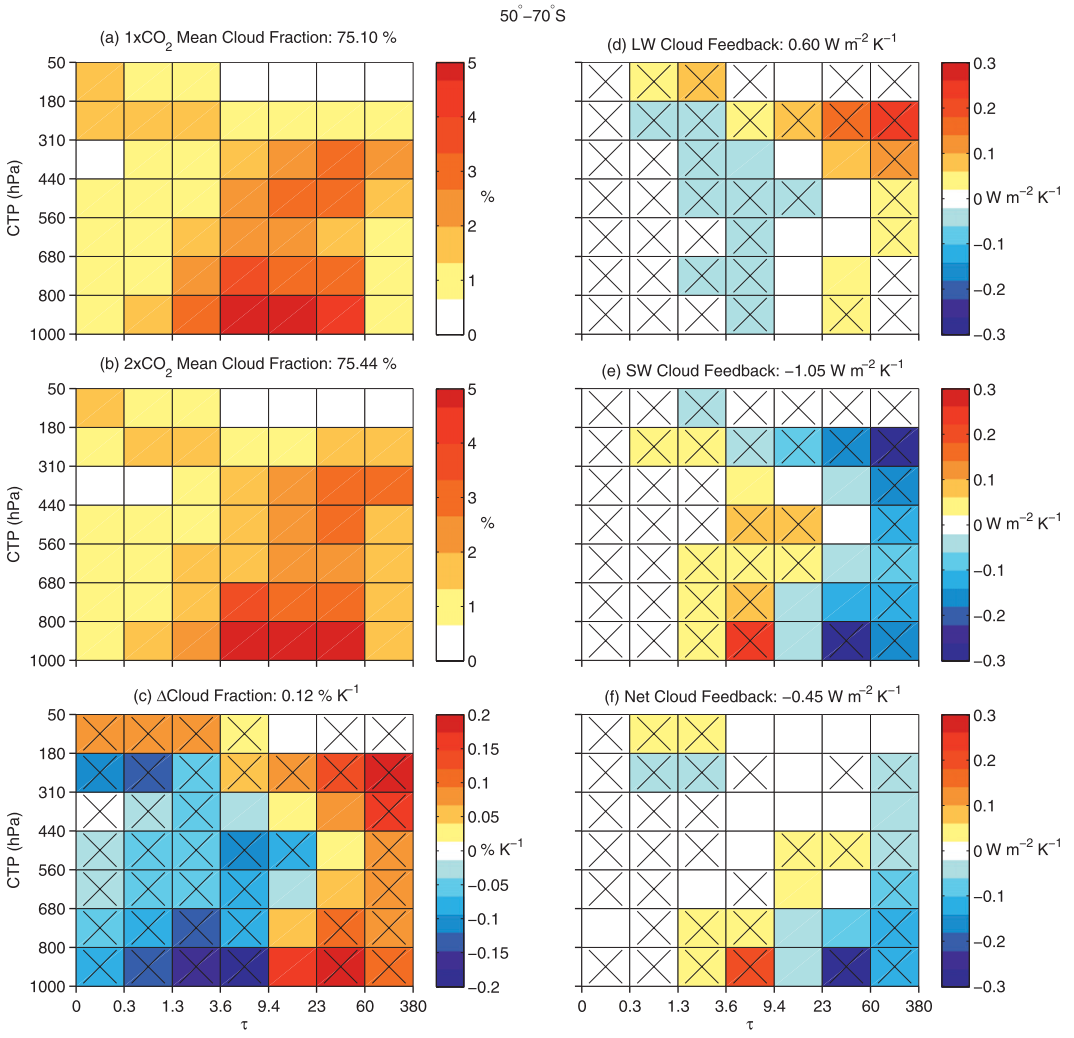


FIG. 7. As in Fig. 6, but for the 50°–70°S region.

to the global and ensemble mean positive LW cloud feedback is the upward shift of clouds, and increases in cloud-top altitude contribute positively in all models, with values spanning a range of 0.68 from 0.05 to 0.73 W m^{-2} K^{-1}. Increases in cloud optical depth contribute positively to the LW cloud feedback in all models, with values spanning a range of 0.58 from 0.02 to 0.60 W m^{-2} K^{-1}. The LW cloud feedback arising from residuals in the change in cloud fraction decomposition spans a range of 0.58 from −0.47 to 0.12 W m^{-2} K^{-1}.

Even though LW cloud feedback is positive in all but one model, it is clear that the relative contributions of cloud amount changes (negative feedback) and cloud altitude changes (positive feedback) vary significantly among models, causing this feedback to exhibit significant spread. For example, models such as the Canadian Centre for Climate Modelling and Analysis fourth-generation atmospheric general circulation model (CCCma AGCM4) and the NCAR Community Climate System Model, version 3 (NCAR CCSM3) have very little cloud amount decrease and a large altitude response, whereas models such as the BMRC1 and the L'Institut Pierre-Simon Laplace Coupled Model, version 4 (IPSL CM4) have the opposite proportionality. Colman and McAvaney (1997) also found a widely varying amount of compensation between these two quantities across four modified versions of the BMRC model, with resultant LW cloud feedbacks of different signs and magnitudes. This demonstrates that large uncertainties remain in the response of clouds relevant to the LW cloud feedback. This, along with the result from Part I that the spread in high-cloud-induced LW and SW cloud feedback estimates exhibits more spread than that due to low clouds, suggests that the community should not focus solely on

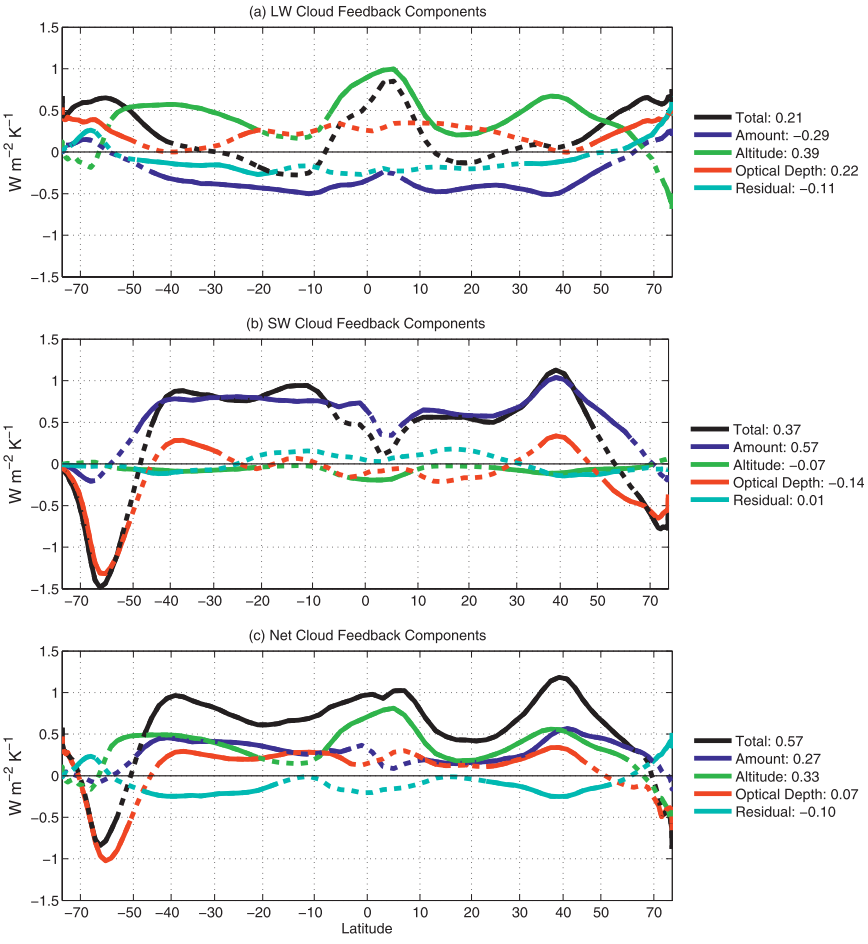


FIG. 8. Zonal, annual, and ensemble mean (a) LW, (b) SW, and (c) net cloud feedbacks partitioned into components due to the change in cloud amount, altitude, and optical depth, and the residual term. Lines are solid where ≥75% of the models agree on the sign of the field plotted, otherwise dashed. The abscissa is the sine of latitude, so that the visual integral is proportional to watts per kelvin of mean surface air temperature change.

the implications of disparate responses of low clouds for cloud feedback.

SW cloud feedback estimates span a range of 1.11 from −0.18 to 0.93 W m^{-2} K^{-1}. Only the GFDL Mixed Layer Model version 2.1 (GFDL MLM2.1), which has the largest negative optical depth feedback, has a negative global mean SW cloud feedback. Decreasing cloud amount makes by far the largest positive contribution to the global and ensemble mean SW cloud feedback, and is the dominant positive contribution in every model except NCAR CCSM3, with values spanning a range of 0.89 from 0.13 to 1.02 W m^{-2} K^{-1}. The range of estimates of this feedback component is the largest of all components among both the SW and LW cloud feedbacks. Increases in cloud-top altitude contribute negatively to the SW cloud feedback in all models, but the values are very small, with none exceeding −0.12 W m^{-2} K^{-1}. SW optical depth feedback estimates, which span a range of 0.69 from −0.55 to 0.14 W m^{-2} K^{-1}, are the only LW or SW nonresidual contributions for which the signs are not consistent across the ensemble. The SW cloud feedback arising from residuals in the change in cloud fraction decomposition makes a negligible contribution in the ensemble mean, but it spans a range of 0.55 from −0.21 to 0.33 W m^{-2} K^{-1}.

Net cloud feedback estimates are positive in all models, spanning a range of 0.78 from 0.16 to 0.94 W m^{-2} K^{-1}. In every model, both the cloud amount and cloud altitude feedbacks contribute positively to the net cloud feedback. Cloud amount feedbacks span a range of 0.36 from 0.06 to 0.42 W m^{-2} K^{-1} and cloud altitude feedbacks span a range of 0.57 from 0.05 to 0.61 W m^{-2} K^{-1}. The net optical depth feedback makes a small positive contribution in the global and ensemble mean, but

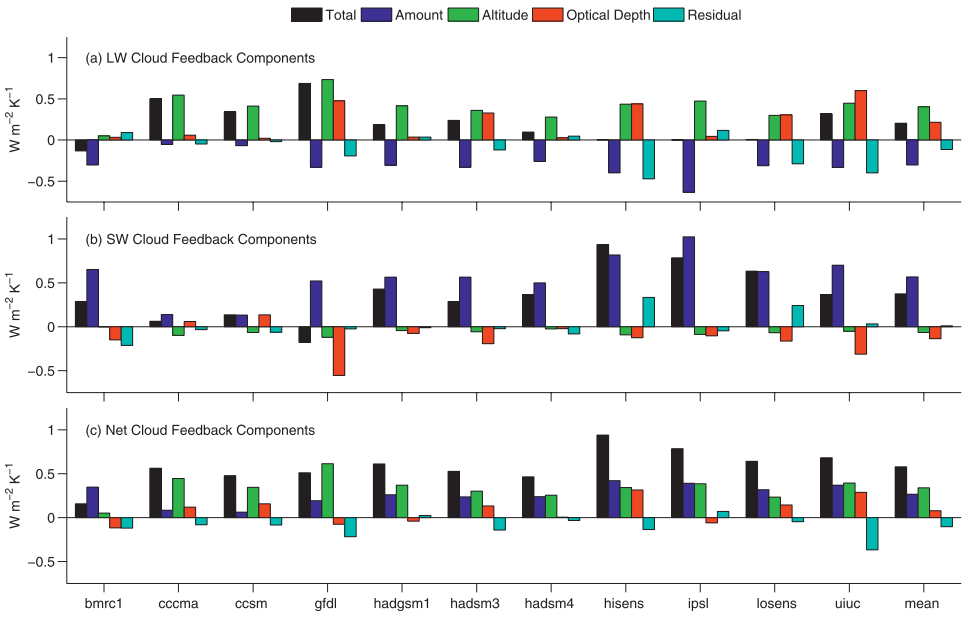


FIG. 9. The (a) LW, (b) SW, and (c) net global and annual mean (black) total, (blue) amount, (green) altitude, (red) optical depth, and (cyan) residual cloud feedbacks estimated for each model.

individual estimates span a range of 0.43 from −0.12 to 0.31 W m^{-2} K^{-1}. The net cloud feedback arising from residuals in the change in cloud fraction decomposition spans a range of 0.44 from −0.37 to 0.07 W m^{-2} K^{-1} and is generally of comparable size to the global mean net optical depth feedback. For every component except altitude, the intermodel spread in net cloud feedback is systematically smaller than for the LW and SW feedbacks, indicating significant anticorrelation across models between LW and SW feedbacks. It is noteworthy that the intermodel spread in the net cloud feedback is smallest for the amount component even though SW amount feedback estimates exhibit the greatest spread of all feedback components. This again argues for caution in interpreting results about the sources of intermodel spread in cloud feedback that only consider the effect of clouds on net radiation.

In most cases, regression coefficients of global mean cloud feedback components on global mean cloud feedback are statistically indistinguishable from zero due to the small sample size of only 11 models. This indicates that intermodel spread is liberally distributed between component changes and LW and SW bands, with no single component playing a dominant role. Two exceptions are the large positive regression coefficients between global mean SW cloud feedback and its amount component (0.58 ±0.34) and between global mean LW cloud feedback and its altitude component (0.57 ±0.25). We also performed a regression of the global mean feedbacks on their values from each grid point, highlighting the local contribution of each process to the spread in global mean cloud feedbacks, but at most locations, the regression slopes are statistically indistinguishable from zero.

6. Conclusions

We have shown a decomposition of the change in cloud fraction histogram that separates cloud changes into components due to the proportionate change in

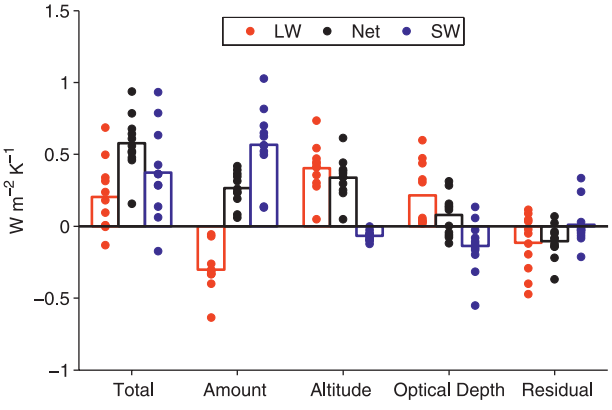


FIG. 10. Global and annual mean (red) LW, (black) net, and (blue) SW cloud feedback estimates and the contribution to the cloud feedbacks from the proportionate change in cloud fraction, change in cloud vertical distribution, change in cloud optical depth distribution, and residual term. Each model is represented by a dot, and the multimodel mean is represented by the height of the vertical bar.

cloud fraction holding the vertical and optical depth distribution fixed, the change in vertical distribution holding the optical depth distribution and total cloud amount fixed, and the change in optical depth distribution holding the vertical distribution and total cloud amount fixed. By multiplying the cloud radiative kernels developed in Part I with these decomposed changes in cloud fraction normalized by the change in global mean surface air temperature, we have computed the cloud amount, altitude, and optical depth feedbacks for an ensemble of 11 models taking part in CFMIP1, allowing us to assess for the first time the relative roles of these processes in determining both the multimodel mean and intermodel spread in LW, SW, and net cloud feedback.

In agreement with many previous studies, a $2 \times CO_2$ climate is associated with a reduction in total cloud amount between about 55°S and 60°N, an increase in cloud amount poleward of these latitudes, an upward shift of cloud tops at nearly every location, an increase in cloud optical depth poleward of about 40°, and a generally much smaller decrease in cloud optical depth equatorward of 40°. We note that changes in both total water path and phase (from ice to liquid) contribute to a shift toward brighter clouds at high latitudes, in agreement with many studies (e.g., Somerville and Remer 1984; Betts and Harshvardan 1987; Tsushima et al. 2006).

Before summarizing our cloud feedback results, we provide two notes of caution. First, our results are derived from an ensemble of 11 global climate models coupled to slab oceans in which CO_2 is instantaneously doubled and the climate is allowed to re-equilibrate. Thus, one should not expect perfect agreement between the estimates of cloud feedback shown here and those presented, for example, in Soden et al. (2008), who analyzed transient climate feedbacks computed as a difference between years 2000 and 2010 and 2090 and 2100 in an ensemble of 14 GCMs coupled to dynamic oceans simulating the Special Report on Emissions Scenarios Special Report on Emissions Scenarios (SRES) A1B scenario. Indeed, here we found a moderately large positive ensemble mean SW cloud feedback of 0.37 W m^{-2} K^{-1} and a LW cloud feedback that is roughly half as large, 0.21 W m^{-2} K^{-1}, whereas these values in GCMs simulating the SRES A2 scenario are 0.09 and 0.49 W m^{-2} K^{-1}, respectively (cf. Fig. 2 of Zelinka and Hartmann 2012). Second, caution is required in interpreting both the mean and intermodel spread in partitioned cloud feedbacks. In the decomposition proposed here, cloud fraction anomalies can ''spread'' throughout the histogram, thereby aliasing, for example, a reduction in low clouds into a positive LW cloud altitude feedback (see section 2). Future work will perform the decomposition of cloud fraction changes in subsections of the ISCCP simulator joint histogram containing similar cloud types, reducing this effect. While the exact values of global mean feedbacks may differ somewhat, we expect that the important processes identified in this study are relevant for other types of model integrations and that other methods of decomposing the cloud distribution changes will lead to similar results.

Rising clouds contribute positively to the LW cloud feedback in every model and represent the dominant contributor to the positive ensemble mean LW cloud feedback, lending further support to the conclusions of Zelinka and Hartmann (2010). Although that study focused solely on the contribution of rising tropical clouds to the positive LW cloud feedback, here we see that rising extratropical clouds make a contribution that is roughly 75% as large as that from tropical clouds. As a deeper troposphere is a consistently modeled and theoretically expected feature of a warmer climate due to increased CO_2, the rise of clouds and its attendant large positive contribution to LW cloud feedback may be considered robust and well explained. The impact of reductions in cloud amount on LW cloud feedback, however, systematically opposes that of increases in cloud altitude, and the ratio of the two components varies considerably among the models, indicating that substantial intermodel variability exists in the response of high clouds, with implications for the size of LW cloud feedback. Nevertheless, in the ensemble mean, the LW cloud amount feedback magnitude is only about 75% as large as the LW cloud altitude feedback. Optical depth increases make a positive contribution to the LW cloud feedback in every model, which, in the ensemble mean, is slightly more than half as large as the LW altitude feedback.

Overall reductions in cloud amount are by far the dominant contributor to the positive SW cloud feedback, and they represent the largest individual contribution to the positive global mean cloud feedback in this ensemble of models. Although this component is positive in every model due to the robust reduction in global mean cloudiness, it exhibits the largest intermodel spread of all feedback components. The positive contribution from cloud amount reductions to SW cloud feedback is roughly twice as large as the magnitude of its negative contribution to LW cloud feedback, highlighting the importance of reductions in low- and midlevel clouds. This factor of 2 is in remarkable agreement with results from both the NCAR model experiment of Taylor and Ghan (1992) and the BMRC model experiment of Colman et al. (2001).

The SW optical depth feedback is small globally, but in every model it is the dominant feedback at high latitudes, where the combination of cloud water content

increases and ice-to-liquid phase changes increases the mean cloud optical depth. That the SW optical depth feedback dominates over the SW cloud amount feedback at high latitudes indicates that increases in the liquid water content of clouds rather than in total cloud amount causes the local SW cloud feedback to be negative. The extent to which cloud brightening is due to dynamics (i.e., thicker cloud types brought to the region by a poleward shift of the storm track) as opposed to thermodynamics (i.e., an increase in the adiabatic water content and/or phase change from ice to liquid in clouds that are already present in the region) remains to be investigated.

Our results clearly show that the net cloud feedback represents the integrated effect of large, spatially heterogeneous—and, in many cases—opposing effects on the radiation budget. Nevertheless, it is positive in every model, as are the contributions from decreasing cloud amount and increasing cloud altitude. Interestingly, increasing cloud altitude makes a larger contribution to net cloud feedback than does decreasing cloud amount, and does so in 8 out of 11 models. This is because LW and SW cloud amount feedbacks tend to offset each other, whereas cloud altitude increases have large positive impacts on LW fluxes that are not significantly opposed in the SW. Although only four models have negative global mean net optical depth feedbacks, all the models exhibit large negative optical depth feedbacks at high latitudes. This locally large negative feedback is primarily due to low clouds becoming thicker, since the increased optical depth of high clouds has compensating effects on LW and SW radiation.

Acknowledgments. We acknowledge the international modeling groups, the Program for Climate Model Diagnosis and Intercomparison (PCMDI), and the WCRP's Working Group on Coupled Modelling (WGCM) for their roles in making available the WCRP CFMIP multimodel dataset. Support of this dataset is provided by the Office of Science, U.S. Department of Energy. We thank Karen Shell and one anonymous reviewer for their detailed critiques of this manuscript; Brian Soden for providing radiative kernels; Rick Hemler for providing additional GFDL MLM2.1 model output; Rob Wood, Chris Bretherton, and Robert Pincus for the useful discussion and their suggestions for improvement; and Marc Michelsen for computer support. This research was supported by the Regional and Global Climate Modeling Program of the Office of Science at the U. S. Department of Energy and by NASA Grant NNX09AH73G at the University of Washington. This work was performed under the auspices of the U.S. Department of Energy by Lawrence Livermore National Laboratory under Contract DE-AC52-07NA27344.

REFERENCES

Betts, A. K., and Harshvardan, 1987: Thermodynamic constraint on the cloud liquid water feedback in climate models. *J. Geophys. Res.,* **92D,** 8483–8485.

Bony, S., and J.-L. Dufresne, 2005: Marine boundary layer clouds at the heart of tropical cloud feedback uncertainties in climate models. *Geophys. Res. Lett.,* **32,** L20806, doi:10.1029/2005GL023851.

——, ——, H. Le Treut, J.-J. Morcrette, and C. Senior, 2004: On dynamic and thermodynamic components of cloud changes. *Climate Dyn.,* **22,** 71–68.

——, and Coauthors, 2006: How well do we understand and evaluate climate change feedback processes? *J. Climate,* **19,** 3445–3482.

Cess, R. D., 1974: Radiative transfer due to atmospheric water vapor: Global considerations of the earth's energy balance. *J. Quant. Spectrosc. Radiat. Transfer,* **14,** 861–871.

——, 1975: Global climate change: An investigation of atmospheric feedback mechanisms. *Tellus,* **27,** 193–198.

——, and Coauthors, 1989: Interpretation of cloud-climate feedback as produced by 14 atmospheric general circulation models. *Science,* **245,** 513–516.

——, and Coauthors, 1990: Intercomparison and interpretation of climate feedback processes in 19 atmospheric general circulation models. *J. Geophys. Res.,* **95** (D10), 16 601–16 615.

Chang, F.-L., and J. A. Coakley, 2007: Relationships between marine stratus cloud optical depth and temperature: Inferences from AVHRR observations. *J. Climate,* **20,** 2022–2036.

Colman, R., 2003: A comparison of climate feedbacks in general circulation models. *Climate Dyn.,* **20,** 865–873.

——, and B. McAvaney, 1997: A study of general circulation model climate feedbacks determined from perturbed sea surface temperature experiments. *J. Geophys. Res.,* **102D,** 19 383–19 402.

——, J. Fraser, and L. Rotstayn, 2001: Climate feedbacks in a general circulation model incorporating prognostic clouds. *Climate Dyn.,* **18,** 103–122.

Feigelson, E. M., 1978: Preliminary radiation model of a cloudy atmosphere. Part I: Structure of clouds and solar radiation. *Beitr. Phys. Atmos.,* **51,** 203–229.

Hall, N. M. J., B. J. Hoskins, P. J. Valdes, and C. A. Senior, 1994: Storm tracks in a high-resolution GCM with doubled carbon dioxide. *Quart. J. Roy. Meteor. Soc.,* **120,** 1209–1230.

Hansen, J., A. Lacis, D. Rind, G. Russell, P. Stone, I. Fung, R. Ruedy, and J. Lerner, 1984: Climate sensitivity: Analysis of feedback mechanisms. *Climate Processes and Climate Sensitivity, Geophys. Monogr.,* Vol. 29, Amer. Geophys. Union, 130–163.

Harrop, B. E., and D. L. Hartmann, 2012: Testing the role of radiation in determining tropical cloud-top temperature. *J. Climate,* in press.

Hartmann, D. L., and K. Larson, 2002: An important constraint on tropical cloud - climate feedback. *Geophys. Res. Lett.,* **29,** 1951, doi:10.1029/2002GL015835.

Klein, S. A., and C. Jakob, 1999: Validation and sensitivities of frontal clouds simulated by the ECMWF model. *Mon. Wea. Rev.,* **127,** 2514–2531.

Kuang, Z., and D. L. Hartmann, 2007: Testing the fixed anvil temperature hypothesis in a cloud-resolving model. *J. Climate,* **20,** 2051–2057.

Kushner, P. J., I. M. Held, and T. L. Delworth, 2001: Southern Hemisphere atmospheric circulation response to global warming. *J. Climate,* **14,** 2238–2249.

Lacis, A., J. Hansen, P. Lee, T. Mitchell, and S. Lebedeff, 1981: Greenhouse effect of trace gases, 1970–1980. *Geophys. Res. Lett.,* **8,** 1035–1038.

Lin, W. Y., and M. H. Zhang, 2004: Evaluation of clouds and their radiative effects simulated by the NCAR Community Atmospheric Model against satellite observations. *J. Climate,* **17,** 3302–3318.

Lorenz, D. J., and E. T. DeWeaver, 2007: Tropopause height and zonal wind response to global warming in the IPCC scenario integrations. *J. Geophys. Res.,* **112,** D10119, doi:10.1029/2006JD008087.

Mace, G. G., E. E. Clothiaux, and T. P. Ackerman, 2001: The composite characteristics of cirrus clouds: Bulk properties revealed by one year of continuous cloud radar data. *J. Climate,* **14,** 2185–2203.

Meehl, G. A., and Coauthors, 2007: Global climate projections. *Climate Change 2007: The Physical Science Basis,* S. Solomon et al., Eds., Cambridge University Press, 747–846.

Mitchell, J. F. B., C. A. Senior, and W. J. Ingram, 1989: CO_2 and climate: A missing feedback? *Nature,* **341,** 132–134.

Paltridge, G. W., 1980: Cloud-radiation feedback to climate. *Quart. J. Roy. Meteor. Soc.,* **106,** 895–899.

Ringer, M. A., and Coauthors, 2006: Global mean cloud feedbacks in idealized climate change experiments. *Geophys. Res. Lett.,* **33,** L07718, doi:10.1029/2005GL025370.

Roeckner, E., U. Schlese, J. Biercamp, and P. Liewe, 1987: Cloud optical depth feedback and climate modeling. *Nature,* **329,** 138–139.

Santer, B. D., and Coauthors, 2003: Contributions of anthropogenic and natural forcing to recent tropopause height changes. *Science,* **301,** 479–483.

Schlesinger, M. E., 1988: Negative or positive cloud optical depth feedback? *Nature,* **335,** 303–304.

Schneider, S. H., 1972: Cloudiness as a global climatic feedback mechanism: The effects on radiation balance and surface temperature of variations in cloudiness. *J. Atmos. Sci.,* **29,** 1413–1422.

——, and R. E. Dickinson, 1974: Climate modeling. *Rev. Geophys.,* **12,** 447–493.

——, W. M. Washington, and R. M. Chervin, 1978: Cloudiness as a climatic feedback mechanism: Effects on cloud amounts of prescribed global and regional surface temperature changes in the NCAR GCM. *J. Atmos. Sci.,* **35,** 2207–2221.

Senior, C. A., and J. F. B. Mitchell, 1993: Carbon dioxide and climate: The impact of cloud parameterization. *J. Climate,* **6,** 393–418.

Soden, B. J., and I. M. Held, 2006: An assessment of climate feedbacks in coupled ocean–atmosphere models. *J. Climate,* **19,** 3354–3360.

——, and G. A. Vecchi, 2011: The vertical distribution of cloud feedback in coupled ocean-atmosphere models. *Geophys. Res. Lett.,* **38,** L12704, doi:10.1029/2011GL047632.

——, I. M. Held, R. Colman, K. M. Shell, J. T. Kiehl, and C. A. Shields, 2008: Quantifying climate feedbacks using radiative kernels. *J. Climate,* **21,** 3504–3520.

Somerville, R. C. J., and L. A. Remer, 1984: Cloud optical thickness feedbacks in the CO_2 climate problem. *J. Geophys. Res.,* **89** (D6), 9668–9672.

Stephens, G. L., 1978: Radiation profiles in extended water clouds. Part II: Parameterization schemes. *J. Atmos. Sci.,* **35,** 2123–2132.

Taylor, K. E., and S. J. Ghan, 1992: An analysis of cloud liquid water feedback and global climate sensitivity in a general circulation model. *J. Climate,* **5,** 907–919.

Tompkins, A. M., and G. C. Craig, 1999: Sensitivity of tropical convection to sea surface temperature in the absence of large-scale flow. *J. Climate,* **12,** 462–476.

Trenberth, K. E., and J. T. Fasullo, 2010: Simulation of present-day and twenty-first-century energy budgets of the southern oceans. *J. Climate,* **23,** 440–454.

Tselioudis, G., and W. B. Rossow, 1994: Global, multiyear variations of optical thickness with temperature in low and cirrus clouds. *Geophys. Res. Lett.,* **21,** 2211–2214.

——, ——, and D. Rind, 1992: Global patterns of cloud optical thickness variation with temperature. *J. Climate,* **5,** 1484–1495.

——, A. D. D. Genio, W. Kovari, and M.-S. Yao, 1998: Temperature dependence of low cloud optical thickness in the GISS GCM: Contributing mechanisms and climate implications. *J. Climate,* **11,** 3268–3281.

Tsushima, Y., and Coauthors, 2006: Importance of the mixed-phase cloud distribution in the control climate for assessing the response of clouds to carbon dioxide increase: A multi-model study. *Climate Dyn.,* **27,** 113–126.

Twomey, S., 1977: The influence of pollution on the shortwave albedo of clouds. *J. Atmos. Sci.,* **34,** 1149–1152.

Vavrus, S., D. Waliser, A. Schweiger, and J. Francis, 2009: Simulations of 20th and 21st century Arctic cloud amount in the global climate models assessed in the IPCC AR4. *Climate Dyn.,* **33,** 1099–1115.

Weaver, C. P., 2003: Efficiency of storm tracks an important climate parameter? The role of cloud radiative forcing in poleward heat transport. *J. Geophys. Res.,* **108,** 4018, doi:10.1029/2002JD002756.

Webb, M. J., C. Senior, S. Bony, and J. J. Morcrette, 2001: Combining ERBE and ISCCP data to assess clouds in the Hadley Centre, ECMWF and LMD atmospheric climate models. *Climate Dyn.,* **17,** 905–922.

——, and Coauthors, 2006: On the contribution of local feedback mechanisms to the range of climate sensitivity in two GCM ensembles. *Climate Dyn.,* **27,** 17–38.

Wetherald, R. T., and S. Manabe, 1980: Cloud cover and climate sensitivity. *J. Atmos. Sci.,* **37,** 1485–1510.

——, and ——, 1988: Cloud feedback processes in a general circulation model. *J. Atmos. Sci.,* **45,** 1397–1415.

Williams, K., and M. Webb, 2009: A quantitative performance assessment of cloud regimes in climate models. *Climate Dyn.,* **33,** 141–157.

Wu, Y., M. Ting, R. Seager, H.-P. Huang, and M. A. Cane, 2011: Changes in storm tracks and energy transports in a warmer climate simulated by the GFDL CM2.1 model. *Climate Dyn.,* **37,** 53–72, doi:10.1007/s00382-010-0776-4.

Wyant, M. C., C. S. Bretherton, J. T. Bacmeister, J. T. Kiehl, I. M. Held, M. Zhao, S. A. Klein, and B. J. Soden, 2006: A comparison of low-latitude cloud properties and their response to climate change in three AGCMs sorted into regimes using mid-tropospheric vertical velocity. *Climate Dyn.,* **27,** 261–279.

Yin, J. H., 2005: A consistent poleward shift of the storm tracks in simulations of 21st century climate. *Geophys. Res. Lett.,* **32,** L18701, doi:10.1029/2005GL023684.

Zelinka, M. D., and D. L. Hartmann, 2010: Why is longwave cloud feedback positive? *J. Geophys. Res.,* **115,** D16117, doi:10.1029/2010JD013817.

——, and ——, 2011: The observed sensitivity of high clouds to mean surface temperature anomalies in the tropics. *J. Geophys. Res.,* **116,** D23103, doi:10.1029/2011JD016459.

——, and ——, 2012: Climate feedbacks and their implications for poleward energy flux changes in a warming climate. *J. Climate,* **25,** 608–624.

——, S. A. Klein, and D. L. Hartmann, 2012: Computing and partitioning cloud feedbacks using cloud property histograms. Part I: Cloud radiative kernels. *J. Climate,* **25,** 3715–3735.

Zhang, M. H., and Coauthors, 2005: Comparing clouds and their seasonal variations in 10 atmospheric general circulation models with satellite measurements. *J. Geophys. Res.,* **110,** D15S02, doi:10.1029/2004JD005021.